Korean J. Chem. Eng., 38(1), 135-143 (2021)
DOI: 10.1007/s11814-020-0663-6

pISSN: 0256-1115
eISSN: 1975-7220

Facile synthesis of polyethyleneimine@Fe_3O_4 loaded with zirconium for enhanced phosphate adsorption: Performance and adsorption mechanism

Chenghui Ma, Xiaoting Zhang, Kang Wen, Rong Wang†, and Runping Han†

College of Chemistry, Zhengzhou University, Kexue Dadao #100, Zhengzhou, China 450001
(*Received 16 June 2020 • Revised 5 August 2020 • Accepted 17 August 2020*)

Abstract−Coating superparamagnetic iron oxide particles, i.e., Fe_3O_4, as adsorbents have major advantages over bare adsorbents for water treatment. As a versatile material, zirconium has been extensively studied for phosphate removal. In this study, the Fe_3O_4 core was pre-coated with branched polyethyleneimine (PEI) first, and then loaded with zirconium to result in a highly selective adsorbent (i.e., Zr-PEI@Fe_3O_4) for phosphate with a greatly broadened pH range. Scanning electron microscopy (SEM), X-ray photoelectron spectroscopy (XPS), BET surface area, and magnetization were used to characterize the resulting adsorbent and to explore the underlying adsorption mechanism. The adsorption performance of Zr-PEI@Fe_3O_4 toward phosphate was performed by batch experiment. The results showed that Freundlich model better fit the adsorption isotherms, while the Elovich equation better described the kinetic process. The maximum adsorption capacity of dephosphorization 32.2 $mg \cdot g^{-1}$ (according to P element) emerged in the condition of 1.0 $g \cdot L^{-1}$ and pH at 2 with 303 K. The process was spontaneous and endothermic. Zr-PEI@Fe_3O_4 has the potential to remove phosphate from solution due to its easy separation and some good adsorption property.

Keywords: Zr-PEI@Fe_3O_4, Phosphate, Adsorption, Regeneration

INTRODUCTION

Phosphorus (P) is an essential nutrient in the aquatic system. However, nutrient enrichment could lead to eutrophication of water bodies, which has become a challenging environmental problem for many years worldwide. Often, phosphorus is the limiting factor responsible for eutrophication, as nitrogen fluxes to water bodies are usually relatively large [1]. Therefore, it is important to remove phosphorus before agricultural, industrial and municipal wastewaters are released. Numerous techniques have been explored and utilized for phosphorus removal, such as chemical precipitation, ion exchange, biological uptake, and adsorption; each has its advantages under certain conditions [3-5]. Adsorption has been applied in real situations and investigated in laboratories extensively for phosphorus removal because of its relatively low cost, wide availability, and high adsorption capacity [6,7].

With ever-stricter regulations for phosphorous, considerable work has been conducted in developing new adsorbents with higher adsorption capacity, selectivity, and easy regeneration, especially with low concentration of phosphorous [8]. With its electron configuration and hard Lewis acid properties, zirconium (Zr) has proven to be a versatile adsorbent for many environmental contaminants, covering inorganic and organic pollutants [8]. It has been explored for phosphate removal for almost a century. Superparamagnetic iron oxide particles, i.e., Fe_3O_4, as adsorbent support offers obvious advantage over traditional adsorbents on easy adsorbent recovery. There have been many attempts to modify Fe_3O_4 with Zr for phosphate removal using different methods. For example, Zr has been coated on Fe_3O_4 directly or through an intermediate layer by several methods. Modifying Fe_3O_4 directly with Zr has been done by both simple coprecipitation and by slow hydrolysis [9]. However, durability concern might hinder the application of coprecipitation method. For intermediate layer approach, silica has been the most common choice for pre-coating Fe_3O_4 before Zr coating [10,11]. Unfortunately, besides the tedious reaction, strong base might dissolve the silica layer during sorbent regeneration [12]. Fe_3O_4 had also been pre-coated with carbon using a rather complicated method [13]. Polyethyleneimine (PEI) contains abundant amino groups which provide rich binding sites. Thanks to the dual nature of these amino groups, PEI has been explored for binding transition metal ions, such as lead and chromium (VI) ion, or anionic ligands [14,15]. It can provide rich binding sites for zirconium or other metal ions. However, because of its solubility, PEI has to be immobilized on solid support to render the recovery and regeneration. An attempt had already been made to coat Fe_3O_4 directly with PEI for phosphate removal. However, the pH working range was limited for the resulting adsorbent. Fe_3O_4 has also been modified by PEI through an intermediate layer of chitosan for phosphate removal [16]. Effort is still needed to improve the reusability of the resulting adsorbent.

The purpose of this study was to synthesize a Zr-PEI@Fe_3O_4 adsorbent for phosphate removal with high adsorption capacity and selectivity using simple traditional procedures. Furthermore, it can be easily separated from mixtures using magnetic method. Branched PEI can form an excellent intermediate layer by cross-link, which in turn provides sufficient surface area for Zr coating. Fe_3O_4 was prepared by traditional coprecipitation. The resulting magnetic nanoparticles were then coated with PEI using a glutaraldehyde cross-linking method, and finally coated with Zr using a simple reaction plus precipitation. To assess its feasibility, adsorption kinetics, isotherms, and adsorption/desorption cycle of phos-

†To whom correspondence should be addressed.
E-mail: wangjoya@zzu.edu.cn, rphan67@zzu.edu.cn

phate adsorption by the product were investigated. To better understand the adsorption mechanism and the effect of water chemistry, the influences of pH, temperature, coexisting anion/ionic strength on phosphate adsorption were also explored.

MATERIALS AND METHODS

1. Materials

Ferric chloride hexahydrate ($FeCl_3 \cdot 6H_2O$), ferrous chloride tetrahydrate ($FeCl_2 \cdot 4H_2O$), ethanol, glutaraldehyde solution (25% w/w), ammonia solution (25%-28% v/v), sodium chloride, and potassium dihydrogen phosphate (KH_2PO_4) were purchased from Sinopharm Chemical Reagent (Shanghai, China). PEI (branched, MW 10,000) and zirconium oxychloride octahydrate ($ZrOCl_2 \cdot 8H_2O$) were obtained from Aladdin (Shanghai, China). All chemical reagents were analytical grade.

2. Preparation of Zr-PEI@Fe_3O_4

Fe_3O_4 nanoparticles were prepared by traditional coprecipitation. 6.0 g $FeCl_3 \cdot 6H_2O$ and 2.2 g $FeCl_2 \cdot 4H_2O$ were dissolved in 200 mL deionized water. The resulting solution was heated to 60 °C with mechanical stirring. Then, ammonia solution (25%-28% v/v) was added dropwise with constant stirring until pH reached 11. Afterwards, the solution was left to cool to room temperature. The Fe_3O_4 precipitation was collected using a magnet and washed with deionized water and ethanol until pH of the supernatant turned neutral. Then, the product was dried at 80 °C for 12 h.

Although PEI had been immobilized on Fe_3O_4 using a simple coprecipitation method, preliminary experiments showed that the performance of the resulting Zr-PEI@Fe_3O_4 from coating PEI using glutaraldehyde cross-linking method was much better than that using the coprecipitation method, which is understandable since some of the PEI branches might be imbedded into the particles during the coprecipitation process. Therefore, PEI@Fe_3O_4 was prepared by a modified glutaraldehyde cross-linking method [17,18]. 5 g Fe_3O_4 nanoparticles was suspended in 100 mL PEI solution (30 g·L^{-1}) with mechanical stirring for 1 h. Then, 20 mL 5% glutaraldehyde solution was added. After continuing to stir for 2 h, the resulting PEI@Fe_3O_4 particles were recovered using a magnet and washed with deionized water and ethanol. Then, the product was dried at 80 °C for 12 h and weighed.

Zr-PEI@Fe_3O_4 was prepared by simple reaction and precipitation. 3 g $ZrOCl_2 \cdot 8H_2O$ was first dissolved in 125 mL deionized water with mechanical stirring at pH range of 1-2. Then, 5 g PEI@Fe_3O_4 was added and suspended with constant stirring for 1 h. Ammonia solution (25%-28% v/v) was added dropwise until pH of the solution reached 9. The mixture was then aged for 2 h at room temperature. Again, the Zr-PEI@Fe_3O_4 adsorbent was collected using a magnet and washed with deionized water until pH of the supernatant turned neutral. Finally, the product was dried at 80 °C for 12 h and weighed.

3. Characterization of the Products

The saturated magnetization and BET surface area of the bare Fe_3O_4, PEI@Fe_3O_4 and Zr-PEI@Fe_3O_4 particles were determined with a hysteresis loop analyzer (PPMS DynaCool, Quantum Design, USA) and a Micromeritics ASAP 2020 (Micromeritics Instrument, USA), respectively. The surface morphology of the particles was analyzed by scanning electron microscopy (SEM) (Su8020, Tianmei Scientific Instrument, China). The chemical composition on Zr-PEI@Fe_3O_4 particle surface before and after phosphate adsorption was determined by X-ray photoelectron spectroscopy (XPS) (Escalab 250Xi, Thermo Fisher , UK).

4. Adsorption Experiment

Adsorption of phosphate on Zr-PEI@Fe_3O_4 was investigated by batch experiment in 20 mL glass sample vials. Typically, 10 mg Zr-PEI@Fe_3O_4 was added into 10 mL phosphate solution with various concentrations (5-50 mg·L^{-1}). After the capped vials were shaken at 120 rpm and 30 °C for a certain period of time, the adsorbents was separated using a magnet, and the phosphate concentration of the solution was determined by the molybdenum-blue method [18]. Effects of pH (2-12), temperature (20, 30, 40 °C), and the coexisting ion/ionic strength (0-0.20 mol·L^{-1} NaCl and Na_2SO_4) on the adsorption performance were also investigated. The amount of unit adsorption capacity and removal efficiency was calculated by Eq. (1) and (2), respectively.

$$q_e = \frac{V(C_0 - C_e)}{m} \quad (1)$$

$$R = \frac{C_0 - C_e}{C_0} \times 100\% \quad (2)$$

where V is the solution volume in L, C_0 and C_e are the initial and final phosphate concentration in the solution in mg·L^{-1} (according to P, following same), respectively, m is the weight of Zr-PEI@Fe_3O_4, 0.010 g. q_e is the amount of phosphate adsorbed at equilibrium in mg·g^{-1}, R (%) represents the removal efficiency, respectively. All the experiments were performed in duplicate and the mean values were reported.

5. Desorption and Regeneration Experiments

Desorption of adsorbed phosphate from Zr-PEI@Fe_3O_4 was also investigated by batch experiment and this can make the process more economical and useful [19,20]. A typical adsorption/desorption cycle was conducted as follows: after a vial containing 10 mg Zr-PEI@Fe_3O_4 and 10 mL phosphate solution at 50 mg·L^{-1} was shaken at 120 rpm and 30 °C for 8 h, the adsorbents were separated using a magnet, and the phosphate concentration of the resulting solution was determined. The amount of phosphate adsorbed could be calculated subsequently. Then, the collected adsorbents were rinsed with deionized water three times and dried at 80 °C for 12 h. To recover the adsorbed phosphate, 10 mL of 1 mol·L^{-1} NaOH solution and the dried adsorbents was mixed by shaking at 120 rpm and 30 °C for 12 h. Afterwards, the adsorbents were collected, rinsed, and dried again for the next adsorption/desorption cycle. The phosphate concentration in the resulting NaOH solution was determined and used to calculate the amount of recovered/desorbed phosphate. All the experiments were performed in duplicate and the mean values were recorded.

RESULTS AND DISCUSSION

1. Characterization of Materials

1-1. SEM, Magnetic Property and Surface Area of Materials

The determined structural parameters of the adsorbent prod-

Table 1. Structural parameters of the synthesized products

Product	Surface area ($m^2 \cdot g^{-1}$)	Saturated magnetization ($emu \cdot g^{-1}$)	ZrO_2 (wt%)
Fe_3O_4	75.3	67.9	-
PEI@Fe_3O_4	91.0	59.9	-
Zr-PEI@Fe_3O_4	61.2	39.9	14.6

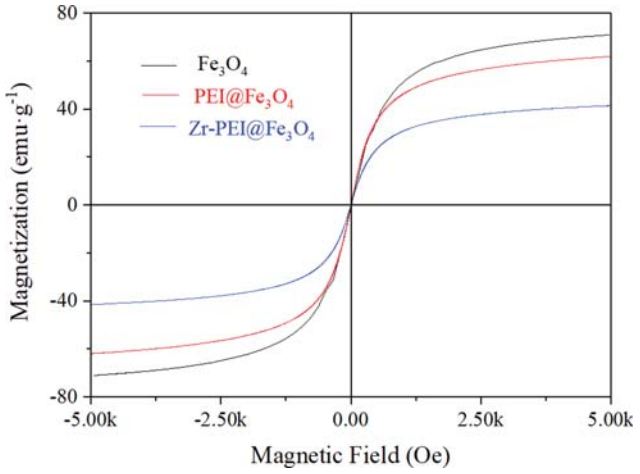

Fig. 1. The hysteresis curves of Fe_3O_4, PEI@Fe_3O_4 and Zr-PEI@Fe_3O_4.

ucts are listed in Table 1. The hysteresis curves of magnetic Fe_3O_4 nanoparticles, PEI@Fe_3O_4 nanoparticles and Zr-PEI@Fe_3O_4 are shown in Fig. 1. The hysteresis curves of Fe_3O_4, PEI@Fe_3O_4, and Zr-PEI@Fe_3O_4 particles confirmed the superparamagnetism of the products. The saturated magnetization value of Fe_3O_4, PEI@Fe_3O_4, and Zr-PEI@Fe_3O_4 particles was 67.9, 59.9, and 39.9 $emu \cdot g^{-1}$, respectively, which reflected a deceasing magnetization after each coating. Meanwhile, the results showed that PEI coating increased the BET surface areas of particles, which might facilitate the Zr loading and phosphate adsorption process [21]. Unfortunately, the Zr coating decreased the BET surface areas of the particles, which might have been caused by aggregated ZrO_2 particles blocking some of the PEI network. The Zr content was estimated as ZrO_2 by the weight difference before and after Zr loading. Zr was loaded onto various supports by either chemical reaction or simple precipitation in the literature [22]. Considering the abundant amino groups and complicated multilayer/branch structure of PEI network, it could take a long time for chemical reaction between Zr and PEI to reach equilibrium, which might subsequently lead to slow phosphate adsorption. Therefore, chemical reaction and precipitation were combined into a simple and efficient process in this study. After Zr(IV) react with PEI network for 1 h, ammonia solution was added to quickly immobilize more Zr onto the PEI branch/network.

The SEM images of PEI@Fe_3O_4, and Zr-PEI@Fe_3O_4 particles are shown in Fig. 2. It was obvious that both products were composed of small particles of irregular shape and different sizes.

1-2. XPS Analysis

The adsorption mechanism was further explored through chemical composition of Zr-PEI@Fe_3O_4 before and after phosphate adsorption using XPS. Fig. 3 shows a new peak at 132.2 eV in wide scan XPS spectrum of Zr-PEI@Fe_3O_4 after phosphate adsorption, which corresponds to P 2p peak with 1.8 eV less than the P 2p peak at 134 eV of standard KH_2PO_4, indicating a strong interaction between Zr and P bonding after the adsorption of phosphate on Zr-PEI@Fe_3O_4 [22,23]. The Zr 3d XPS spectra show noticeable changes before and after phosphate adsorption (Fig. 4(a) and 4(b)). Two peaks at 181.18 and 183.65 eV before phosphate adsorption shifted to 181.34 and 183.72 eV after phosphate adsorption [24], indicating possible electron transfer in the valence band and the formation of Zr-O-P inner-sphere binding, which was also observed in previous studies. The O 1s XPS spectra also show considerable changes before and after phosphate adsorption (Fig. 4(c) and 4(d)). The three peaks at 529.0, 530.6, and 531.8 eV were corresponding to O^{2-} (e.g. Zr-O), OH/O-P binding, and H_2O (adsorbed water), respectively, before phosphate adsorption shifted to 529.8,

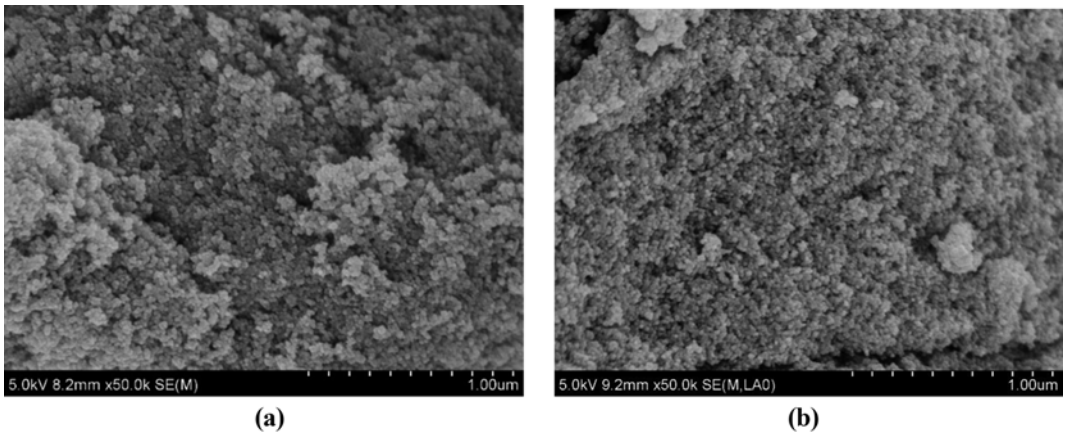

Fig. 2. SEM images of PEI@Fe_3O_4 (a) and Zr-PEI@Fe_3O_4 (b).

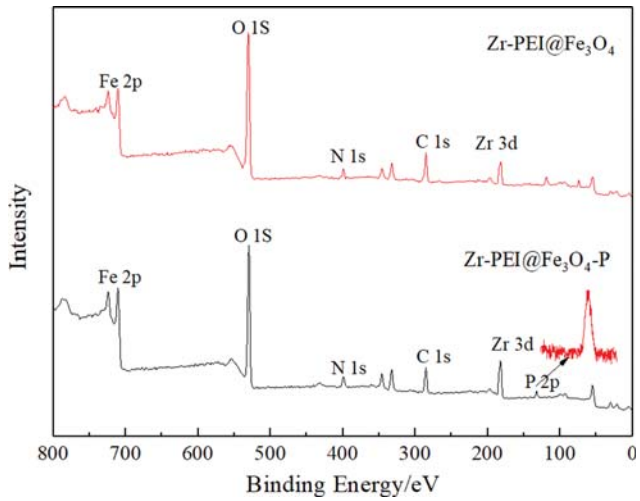

Fig. 3. Wide scan XPS spectra of Zr-PEI@Fe_3O_4 before and after phosphate adsorption.

531.1, and 532.6 eV after phosphate adsorption [25]. The fraction of the OH/O-P component increased from 23.6% to 31.7%, while the O^{2-} and H_2O components decreased from 58.5% and 17.9% to 55.7% and 12.5%, respectively. Similar findings have also been observed in previous studies, which might indicate the formation of O-P bonding on Zr-PEI@Fe_3O_4 [26].

XPS spectra analysis confirms that the strong complexation between Zr and phosphate plays an important role in phosphate adsorption on Zr-PEI@Fe_3O_4, in line with previous studies [27,28]. Meanwhile, experimental results also show that electrostatic interaction and ion exchange contribute to the adsorption process. Based on the rapid phosphate removal by Zr-PEI@Fe_3O_4 at low phosphate concentration, the sufficient surface area of the ZrO_2 on the out-layer of the PEI network provides abundant binding sites for phosphate at low concentration.

2. Adsorption Study

2-1. Effect of pH and Coexisting Anions on Adsorption

Fig. 5 shows the effect of solution pH on phosphate adsorption by Zr-PEI@Fe_3O_4 at the initial concentration of 50 mg·L^{-1}. As pH value increases from 2 to 12, phosphate adsorption decreases from 34.9 mg·g^{-1} to 11.3 mg·g^{-1}. This trend has been well documented and could be easily explained with electrostatic interaction mechanism [29]. With lower pH, more hydroxyl groups at the surface of Zr-PEI@Fe_3O_4 particles become protonated and carry positive charges, which facilitates the adsorption of the negative charged phosphate ions [30]. With the ongoing of pH, Zr-PEI@Fe_3O_4 had little effect on phosphorus removal, indicating that the electrostatic attraction interaction was unlikely to be the main mechanism of

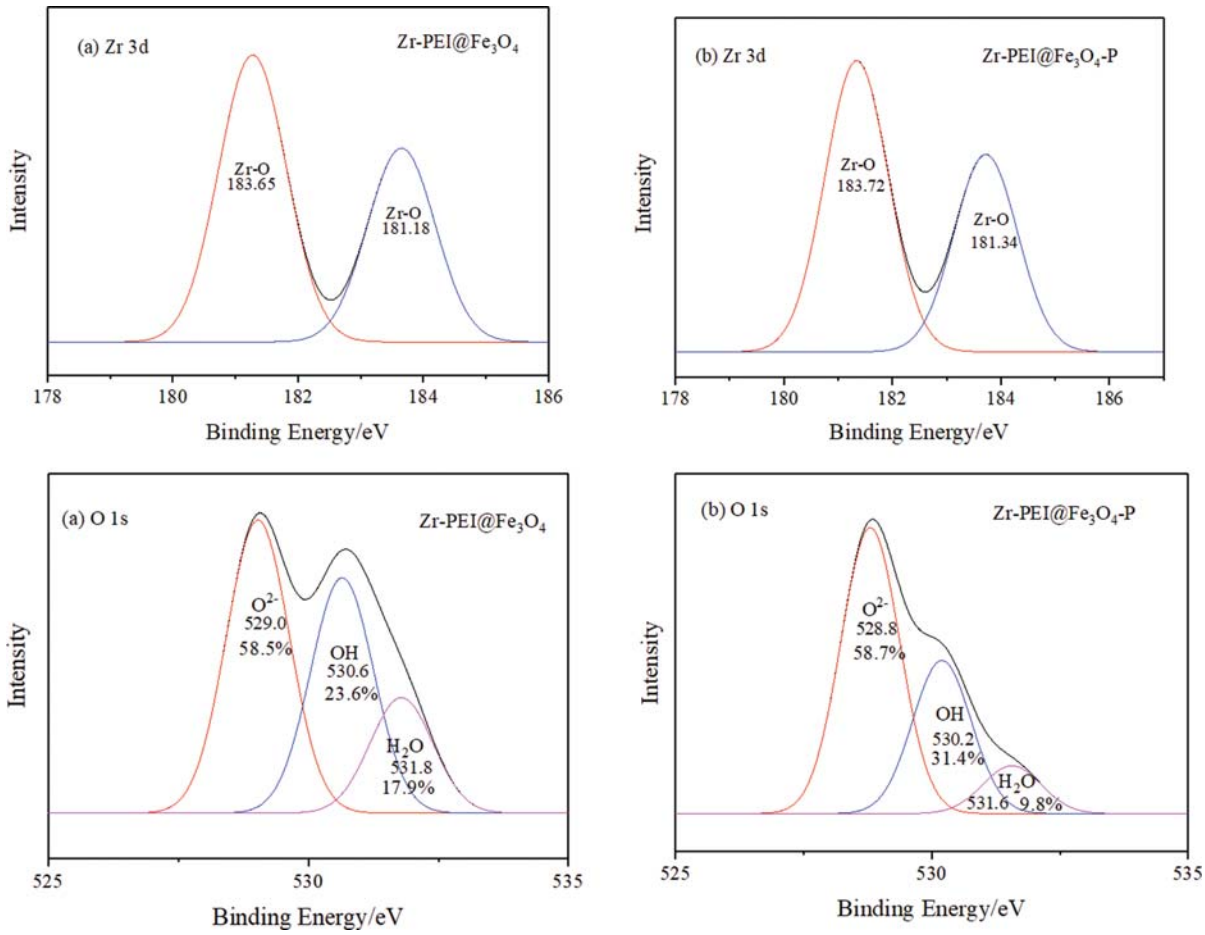

Fig. 4. High-resolution Zr 3d and O1s XPS before and after adsorption of phosphate.

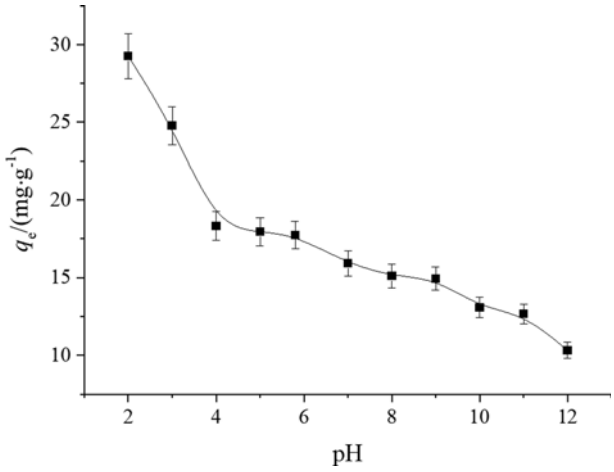

Fig. 5. Effect of pH on phosphate adsorption.

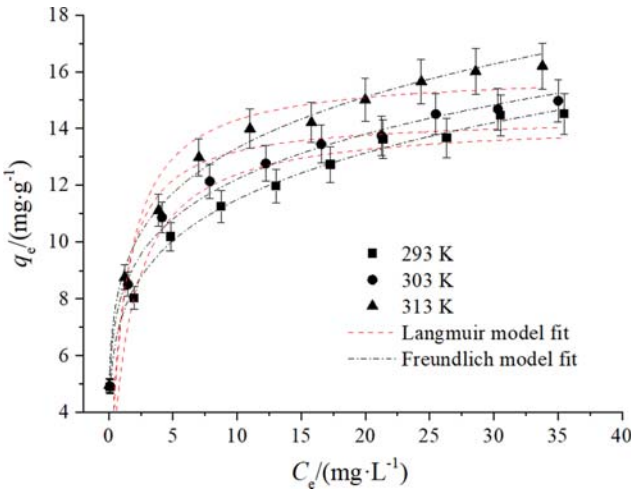

Fig. 7. Adsorption isotherms of phosphate adsorption onto Zr-PEI@Fe_3O_4 (pH=6.0).

phosphate adsorption. As described elsewhere, the surface charge of the adsorbent has a certain effect on phosphate adsorption, but it does not rely on static electricity entirely [31]. In this pH, ion exchange may play a leading role in phosphate adsorption. The main mechanism of action of zirconium oxide on phosphate adsorption was anion coordination exchange, which means the complex formation generated with phosphate in water [32], the adsorption was optimal as the solution pH=2 within the pH range tested. Considering the practical application and the utilization of the adsorbent, the pH of the solution was chosen to be 6.0 and used for subsequent studies.

Selectivity is an essential attribute for a competent adsorbent. Therefore, the effect of competitive common anions on phosphate adsorption by Zr-PEI@Fe_3O_4 was investigated. Fig. 6 shows that at pH=6, chloride ion and sulfate ion have a slight negative effect, and sulfate had a greater effect on adsorption than chloride ion. This may be caused by the electrostatic adsorption of phosphate by Zr-PEI@Fe_3O_4. However, when the anion concentration was increased, there was little effect on the adsorption, probably because an inter-

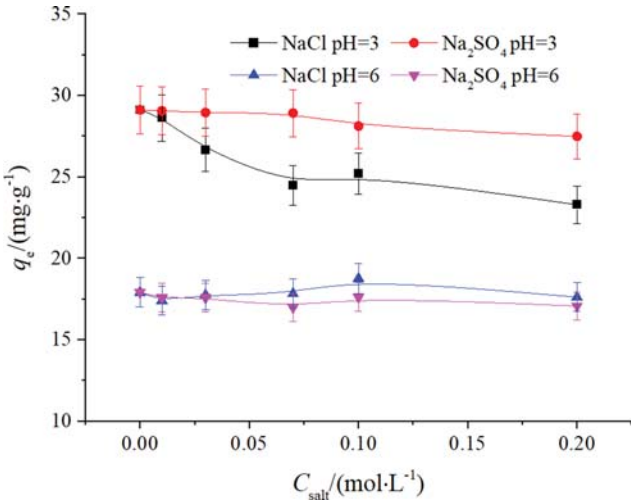

Fig. 6. Effect of coexisting anions on phosphate adsorption.

nal layer complex was formed between Zr-PEI@Fe_3O_4 and the phosphate. Compared with pH 6, when the solution pH is 3, with the increase of ion concentration, the adsorption capacity of Zr-PEI@Fe_3O_4 on phosphate ions decreases significantly and the influence of sulfate ions is greater, which indicates that Zr-PEI@Fe_3O_4 has an inhibitory effect on the adsorption of phosphorus under acidic conditions. With the increasing of pH value, the inhibition of Zr-PEI@Fe_3O_4 adsorption capacity was very limited. In general, Zr-PEI@Fe_3O_4 had good ion selectivity. In following study, solution pH was adjusted to 6.0 as pH of the practical wastewater is often near neutral.

2-2. Adsorption Isotherm Analysis

The adsorption isotherm indicates that the distribution of the adsorbate molecules between the liquid phase and the solid phase was obtained by changing the initial concentration of P (5-50 mg·L^{-1}) at a given pH and temperature [33,34]. The results are presented in Fig. 7, which clearly shows that the adsorption capacity increased with increasing temperature and this indicated that the adsorption of phosphate by Zr-PEI@Fe_3O_4 was endothermic. At the same temperature, values of q_e became larger with the increase of equilibrium concentration, up to near little of change of q_e at higher range of concentration. It was also observed that there was still some adsorption quantity at lower equilibrium. So it can be implied that the equilibrium concentration is near zero when initial concentration is lower than 2 mg·L^{-1} (value of q_e is to 2.0 mg·g^{-1} and the equilibrium time is only 3 min at 303 K). This showed that there was some competitive and advantage in removal of lower phosphate concentration from solution.

The experimental data were fitted and analyzed using the Freundlich model and Langmuir model (expressions listed in Table 2). The model fitted the experimental data to the adsorption isotherms and isotherms constants as shown in Fig. 7 and Table 3, respectively. The data had a high correlation determined coefficient (R^2) with the Freundlich model. The adsorption of phosphate was more inclined towards the Freundlich model which belonged to the multiphase multi-molecular layer adsorption process. Moreover, it can be seen from the data fitted by the Freundlich model

Table 2. Several common adsorption models

Models	Nonlinear form	Symbol description
Isotherm model		
Langmuir	$q_e=\frac{q_m K_L c_e}{1+K_L c_e}$	q_m (mg·g^{-1}) is monolayer theoretical saturated adsorption amount; K_L (L·mg^{-1}) is constant associated with binding energy.
Freundlich	$q_e=K_F c_e^{1/n}$	K_F and 1/n are temperature dependent constants.
Kinetic model		
Pseudo-second-order kinetic model	$q_t=\frac{k_2 q_e^2 t}{1+k_2 q_e t}$	k_2 (g·mg^{-1}·min^{-1}) is a quasi-secondary rate constant.
Elovich equation	$q_t=A+B\ln t$	A and B are constants.

Table 3. Fitting results of adsorption isotherm models

Langmuir					
T/K	K_L/(L·mg^{-1})	$q_{e(exp)}$/(mg·g^{-1})	$q_{m(theo)}$/(mg·g^{-1})	R^2	SSE
293	0.111±0.024	14.5	11.8±0.9	0.962	2.46
303	0.145±0.035	15.0	13.5±1.1	0.955	4.17
313	0.147±0.036	16.4	14.7±1.2	0.955	5.09
Freundlich					
T/K	K_F	1/n		R^2	SSE
293	2.17±0.15	0.434±0.024		0.987	0.833
303	2.91±0.07	0.410±0.009		0.998	0.201
313	3.18±0.08	0.413±0.009		0.998	0.240

Note: SSE=$\Sigma(q-q_c)^2$, q and q_c are the experimental value and calculated value according to the model, respectively.

Table 4. Fitting results of adsorption kinetic models

Elovich equation					
T/K	C_0/(mg·L^{-1})	A	B	R^2	SSE
293	15	2.90±0.17	1.31±0.08	0.969	0.649
	30	3.37±0.34	1.54±0.07	0.980	0.579
	50	10.3±0.2	0.789±0.05	0.963	0.283
303	15	4.32±0.19	0.967±0.042	0.983	0.191
	30	5.67±0.30	3.37±0.34	0.974	0.442
	50	10.4±0.2	1.01±0.04	0.986	0.171
313	15	4.40±0.126	1.039±0.027	0.994	0.0802
	30	5.69±0.3	1.17±0.06	0.973	0.447
	50	10.7±0.3	1.01±0.05	0.974	0.316
Pseudo-second-order kinetic model					
T/K	C_0/(mg·L^{-1})	$q_{e(exp)}$/(mg·g^{-1})	$q_{e(theo)}$/(mg·g^{-1})	k_2/(g·mg^{-1}·min^{-1})	R^2	SSE
293	15	10.2	10.0±0.1	6.17E-2±0.01E-2	0.913	94.9
	30	12.4	12.0±0.4	0.0084±0.0018	0.863	3.92
	50	15.0	14.6±0.2	0.0271±0.0048	0.832	1.26
303	15	10.4	10.1±0.1	0.0165±0.0021	0.936	0.714
	30	12.3	12.1±0	0.929E-2±0.015E-2	0.878	106
	50	16.0	15.7±0.2	0.0194±0.0028	0.897	1.26
313	15	10.6	10.1±0.2	0.0154±0.0031	0.849	1.94
	30	12.6	12.5±0.2	0.0138±0.0023	0.888	1.85
	50	16.5	16.2±0.2	0.0195±0.0025	0.911	1.09

that 1/n between 0 and 0.5 indicates that Zr-PEI@Fe_3O_4 has a better adsorption effect on phosphate.

2-3. Adsorption Kinetics Analysis

Adsorption rate is an important property of adsorbents. The adsorption performance of PEI@Fe_3O_4 and Zr-PEI@Fe_3O_4 toward phosphate was studied experimentally, which proved that Zr-PEI@Fe_3O_4 has good adsorption performance. The adsorption kinetics of phosphate on Zr-PEI@Fe_3O_4 as a function of temperature is shown in Fig. 8. At different temperatures, the initial phosphate concentration was 50 mg·L^{-1}, the adsorption process mainly included rapid growth in 100 min, increased in 100-250 min slowly and equilibrium in 360 min. This phenomenon means that there were sufficient adsorption sites on the surface of the adsorbent, and the adsorption speed was faster; as the active sites on the adsorbent decreased, the relative binding active sites decrease and the adsorption rate became slower [35]. The adsorption quantity was 16.0 mg·g^{-1} at 303 K.

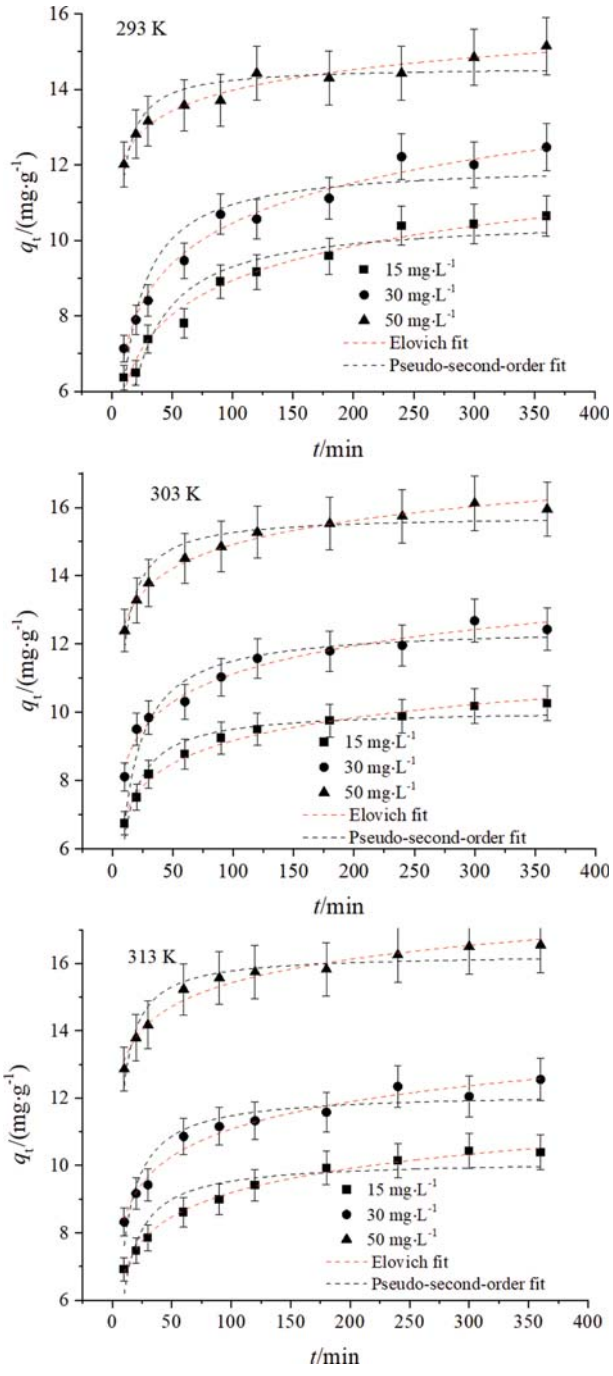

Fig. 8. Adsorption kinetics of phosphate adsorption onto Zr-PEI@Fe_3O_4 (pH=6.0).

At 303 K, the adsorption quantity of PEI@Fe_3O_4 toward phosphate was 14.0 mg·g^{-1} (at pH 6.0). Furthermore, adsorption quantity of phosphate onto PEI@Fe_3O_4 significantly decreased if there was higher concentration of existing common salts. So it was valuable to explore the adsorption property of Zr-PEI@Fe_3O_4 for removal of phosphate from solution.

To study the adsorption kinetics in-depth, the two kinetic equations (expressions listed in Table 2) of the Elovich equation and pseudo-second-order kinetic model were selected and nonlinear regression analysis was applied to fit the experimental data [36,37]. The fitting curve and fitting parameters are shown in Fig. 8 and Table 4, respectively. The values of $q_{e(theo)}$ from Pseudo-second-order kinetic model were close to values of $q_{e(exp)}$ from experiments and this indicated that the pseudo-second-order kinetic model was used to predict the equilibrium adsorption amount. But the values of R^2 were lower, which was not suitable for describing the whole kinetic process of phosphate adsorption onto Zr-PEI@Fe_3O_4. The Elovich equation model had a higher R^2 value (>0.96) and a lower *SSE* value. The parameter A increased with the increase of the initial concentration which indicated that the adsorption process contains heterogeneous chemical adsorption and ion exchange.

2-4. Adsorption Thermodynamic Parameters

The adsorption process was accompanied by the characteristics of endothermic, exothermic, adsorption force and system changes. The mechanism of adsorption reaction can be inferred from the perspective of energy change, so it can be passed by Gibbs free energy (ΔG), enthalpy change (ΔH), and entropy change (ΔS) [38]. Analytical calculations were performed with the following formula [39]:

$$K_c = C_{ad,e}/C_e \quad (3)$$

$$\Delta G = -RT\ln K_c \quad (4)$$

$$\Delta G = \Delta H - T\Delta S \quad (5)$$

where K_c is the adsorption equilibrium constant, $C_{ad,e}$ (mg·L^{-1}) and C_e (mg·L^{-1}) are the concentration of the adsorbate on the adsorbent and the concentration of the adsorbate in the solution when the adsorption is balanced. ΔG represents the Gibbs free energy; R (8.314 J·mol^{-1}·K^{-1}) denotes the gas constant; T (K) expresses the absolute temperature;

For the actual system, in addition to considering the possibility of reaction, the reaction rate should also be considered. It can be expressed by activation energy. The apparent activation energy can be obtained by bringing the most consistent kinetic adsorption model parameters into the Arrhenius equation:

$$\ln k = -\frac{E_a}{RT} + \ln A \quad (6)$$

where k is the adsorption rate constant, E_a (kJ·mol^{-1}) represents

Table 5. Thermodynamic parameters

E_a/(kJ·mol^{-1})	ΔH/(kJ·mol^{-1})	ΔS/(J·mol^{-1}·K^{-1})	ΔG/(kJ·mol^{-1})		
			293 K	303 K	313 K
29.9	134	38.5	−9.33	−11.7	−12.0

Table 6. Comparison of adsorption quantity of phosphate onto various adsorbents

Adsorbent	q_e (mg·g^{-1})	Reference
Zirconia-modified carbon nanotubes	10.6	[23]
La-modified macroporous chelating resin	26.1	[35]
Fe-IDA-magnetic peanut husk	33.7	[42]
Fe_3O_4@La-Ce composite	56.8	[44]
Zirconia-functionalized graphite oxide	16.4	[46]
Hydrous Zirconium oxide	53.6	[47]
Fe-modified macroporous chelating resin	10.9	[48]
Zr-PEI@Fe_3O_4	29.8	This study

the apparent activation energy of the reaction, R (8.314 J·mol^{-1}·K^{-1}) denotes the gas constant, T (K) expresses the absolute temperature, and A is the temperature influence factor.

According to Eqs. (3)-(6), the relevant thermodynamic parameters for phosphorus adsorption are calculated and shown in Table 5.

It proved that ΔG was less than zero, drastically suggesting that the driving force of adsorption was greater and the adsorption capacity was higher [40]. ΔH was greater than zero, ΔS was 38.5 J·mol^{-1}·K^{-1}, and the absolute value of ΔG increased with increasing temperature. The adsorption process for phosphate was a spontaneous endothermic reaction from Table 5. The size of the activation energy can judge the difficulty of the adsorption reaction, and the smaller the value the easier the adsorption reaction occurs. From the table, E_a was 29.9 kJ·mol^{-1}, indicating that the reaction was easy to proceed, E_a is between 5 and 40, which indicates that the adsorption process is physical adsorption.

2-5. Desorption of Adsorbed Phosphate and Regeneration of Used Adsorbent

Regeneration of exhausted adsorbent is the critical consideration in the utilization of adsorbent because of cost-effectiveness and concerns of secondary pollution [41-45]. To evaluate the reusability of the Zr-PEI@Fe_3O_4 adsorbent, five phosphate adsorption/desorption cycles were conducted. Thanks to the considerable phosphate adsorption capacity of Zr-PEI@Fe_3O_4 at high pH, such as 11.3 mg g at pH 12, only a very strong base solution might be able to effectively release the adsorbed phosphate from the adsorbent. 1 mol·L^{-1} NaOH solution was used as the desorption solution. The phosphate adsorption capacity remains 80% of the original value after five cycles and the phosphate recovery remains above 70%.

2-6. Comparison of Adsorption Capacity with other Adsorbents Toward Phosphate

Comparison of adsorption capacity with other adsorbent can be performed and this can show the advantage of Zr-PEI@Fe_3O_4. Of course, other factors, such as cost, reuse and effect of common ions also affect the application of adsorbents. Table 6 shows the comparison of phosphate adsorption capacity of Zr-PEI@Fe_3O_4 and other adsorbents. Obviously, the adsorption capacity of Zr-PEI@Fe_3O_4 is greater than that of traditional adsorbent and has a certain practical application prospect.

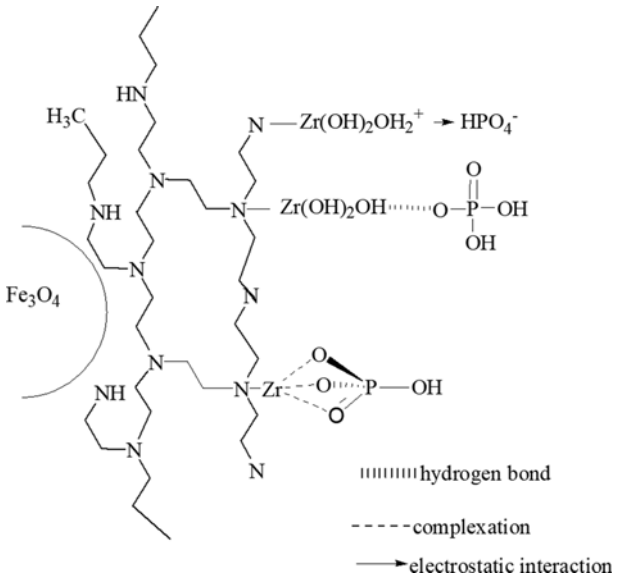

Fig. 9. Plausible mechanism for the adsorption of phosphate over Zr-PEI@Fe_3O_4.

2-7. Adsorption Mechanism

The functional group of PEI contained a large amount of amino groups and more adsorption sites were obtained by binding zirconium on the surface of PEI. The surface of adsorbent is positively charged under acidic conditions. Due to the electrostatic interaction, the phosphate was adsorbed as negative ions. When the pH value increased, the positive charge on the surface of Zr-PEI@Fe_3O_4 decreased gradually, the electrostatic attraction to phosphate decreased. There was still a certain amount of adsorption, indicating that the surface charge of the adsorbent has a certain influence on phosphate adsorption but it does not completely rely on static electricity. The main mechanism of action was to form a complex between ZrO^{2+} and phosphate on surface of adsorbents, also including attraction [49,50]. The mechanism diagram is shown in Fig. 9.

CONCLUSIONS

Via a simple procedure with glutaraldehyde cross-linking and precipitation, PEI and Zr were coated on Fe_3O_4 to produce a selective adsorbent for phosphate removal. There was high adsorption capacity of Zr-PEI@Fe_3O_4 toward phosphate. The adsorption of phosphate by Zr-PEI@Fe_3O_4 involves physical adsorption and heterogeneous chemisorption. The adsorption process is more inclined to the Freundlich isothermal model. The double constant model and Elovich equation model can be used to describe the multi-

phase and multi-molecular layer adsorption process. The adsorption process was spontaneous and endothermic from the thermodynamic analysis. The spent adsorbent could be regenerated using NaOH solution and the adsorption capacity could remain 80% after five adsorption/desorption cycles. In this study, PEI provided a large surface area for Zr coating. Fast adsorption of phosphate and reusability of Zr-PEI@Fe_3O_4 make the adsorbent a potential candidate for phosphate removal.

ACKNOWLEDGEMENT

This work was supported in part by the Key Scientific Research Project in Universities of Henan Province (19A150048).

REFERENCES

1. B. K. Mayer, D. Gerrity, B. E. Rittmann, D. Reisinger and S. Brandt-Williams, *Crit. Rev. Environ. Sci. Technol.*, **43**, 409 (2013).
2. O. Axinte, I. S. Badescu, C. Stroe, V. Neacsu, L. Neacsu and D. Bulgariu, *Environ. Eng. Manage. J.*, **14**, 559 (2015).
3. Y. Yang, X. Shi, W. Ballent and B. K. Mayer, *Water Environ. Res.*, **89**, 2122 (2017).
4. L. H. Peng, H. Dai, Y. Wu, Y. Peng and X. Lu, *Chemosphere*, **197**, 768 (2018).
5. X. Xu, B. Y. Gao, B. Jin and Q. Y. Yue, *J. Mol. Liq.*, **215**, 565 (2016).
6. B. L. Wu, J. Wan, Y. Y. Zhang, B. C. Pan and I. M. C. Lo, *Environ. Sci. Technol.*, **54**, 50 (2020).
7. P. S. Kumar, L. Korving, M. C. M. van Loosdrecht and G. J. Witkamp, *Water Res. X*, **4**, 100029 (2019).
8. A. Bhatnagar, E. Kumar and M. Sillanp, *Chem. Eng. J.*, **171**, 811 (2011).
9. Z. Wang, M. C. Xing, W. K. Fang and D. Y. Wu, *Appl. Surf. Sci.*, **366**, 67 (2016).
10. A. Sarkar, S. K. Biswas and P. Pramanik, *J. Mater. Chem.*, **20**, 4417 (2010).
11. W. J. Wang, J. Zhou, D. Wei, H. Q. Wan, S. R. Zheng, Z. Y. Xu and D. Q. Zhu, *J. Colloid Interface Sci.*, **407**, 442 (2013).
12. L. T. Pham, D. L. Sedlak and F. M. Doyle, *Appl. Catal. B.*, **126**, 258 (2012).
13. W. Wang, H. Zhang, L. Zhang, H. Wan, S. Zheng and Z. Xu, *Colloids Surf. A.*, **469**, 100 (2015).
14. F. An and B. Gao, *J. Hazard. Mater.*, **145**, 495 (2007).
15. B. Y. Huang, Y. G. Liu, B. Li, H. Wang and G. Zeng, *RSC Adv.*, **9**, 32462 (2019).
16. C. C. Fu, H. N. Tran, X. H. Chen and R. S. Juang, *J. Ind. Eng. Chem.*, **11**, 33 (2019).
17. R. P. Han, L. Y. Fang, X. Y. Li, M. Y. Han and Z. Zhang, *J. Zhengzhou U. (Eng. Sci.)*, **40**(2), 59 (2019) (in Chinese).
18. Y. F. Gu, M. Y. Liu, M. M. Yang, W. L. Wang, S. S. Zhang and R. P. Han, *Desalin. Water Treat.*, **138**, 368 (2019).
19. S. Noreen, H. N. Bhatti, M. Iqbal, F. Hussain and F. M. Sarim, *Int. J. Biol. Macromol.*, **147**, 439 (2019).
20. U. Kamran, H. N. Bhatti, M. Iqbal, S. Jamil and M. Zahid, *J. Mol. Struct.*, **1179**, 532 (2019).
21. M. Y. Liu, X. T. Zhang, Z. H. Li, L. B. Qu and R. P. Han, *Carbohyd. Polym.*, **248**, 116792 (2020).
22. Y. F. Gu, M. M. Yang, W. L. Wang and R. P. Han, *J. Chem. Eng. Data*, **64**, 2849 (2019).
23. A. Yuchi, A. Ogiso, S. Muranaka and T. Niwa, *Anal. Chim. Acta*, **494**, 81 (2003).
24. Y. H. He, H. Lin, Y. B. Dong and L. Wang, *Appl. Surf. Sci.*, **426**, 995 (2017).
25. W. Y. Du, Y. Li, X. Xu, Y. A. Shang and B. Y. Gao, *J. Colloid Interface Sci.*, **9**, 2 (2018).
26. J. M. Luo, X. B. Luo, J. Crittenden, J. H. Qu, Y. H. Bai, Y. Peng and J. H. Li, *Environ. Sci. Technol.*, **18**, 1115 (2015).
27. M. Mallet, K. Barthélémy, C. Ruby, A. Renard and S. Naille, *J. Colloid Interface Sci.*, **407**, 95 (2013).
28. L. P. Fang, L. Z. Huang, P. E. Holm, X. F. Yang, H. C. B. Hansen and D. Wang, *J. Mater. Chem. A*, **3**, 75055 (2015).
29. K. Wu, Y. Li, T. Liu, Q. Huang, S. Yang, W. Wang and P. Jin, *Appl. Surf. Sci.*, **478**, 539 (2019).
30. L. G. Yan, Y. Y. Xu, H. Q. Yu, X. D. Xin, Q. Wei and B. Du, *J. Hazard. Mater.*, **179**, 244 (2010).
31. W. W. Huang, S. B. Wang, Z. H. Zhu, L. Li, X. D. Yao, V. Rudolph and F. Haghseresht, *J. Hazard. Mater.*, **158**, 35 (2008).
32. F. Long, J. L. Gong, G. M. Zeng, L. Chen, X. Y. Wang, J. H. Deng, Q. Y. Niu, H. Y. Zhang and X. R. Zhang, *Chem. Eng. J.*, **171**, 448 (2011).
33. Z. M. Ren, L. N. Shao and G. S. Zhang, *Water, Air, Soil Pollut.*, **223**, 4221 (2012).
34. B. L. Zhao, W. Xiao, Y. Shang, H. M. Zhu and R. P. Han, *Arab. J. Chem.*, **10**, s359 (2017).
35. X. T. Zhang, C. H. Ma, K. Wen and R. Han, *Korean J. Chem. Eng.*, **37**, 776 (2020).
36. B. D. Chen, J. Wang, L. J. Kong, X. X. Mai, N. C. Zheng, Q. H. Zhong, J. Y. Liang and D. Y. Chen, *Colloids Surf. A*, **520**, 612 (2017).
37. Y. C. Rong and R. P. Han, *Korean J. Chem. Eng.*, **36**, 942 (2019).
38. Y. Y. Hu and R. P. Han, *J. Chem. Eng. Data*, **64**, 791 (2019).
39. Y. Q. Yang, D. W. Wen, Q. Ding, Y. Wang, N. Liu, Y. Zhao and X. Zhang, *Desalin. Water Treat.*, **88**, 257 (2017).
40. R. D. Zhang, J. H. Zhang, X. N. Zhang, C. C. Dou and R. P. Han, *J. Taiwan Inst. Chem. Eng.*, **45**, 2578 (2014).
41. Z. H. Chen, J. A. Zhang, J. W. Fu, M. H. Wang, X. Z. Wang, R. P. Han and Q. Xu, *J. Hazard. Mater.*, **273**, 263 (2014).
42. A. A. Aryee, F. M. Mpatani, X. T. Zhang, A. N. Kani, E. Dovi, R. P. Han, Z. H. Li and L. B. Qu, *J. Clean. Prod.*, **268**, 122191 (2020).
43. H. N. Bhatti, Y. Safa, S. M. Yakout, O. H. Shair, M. Iqbal and A. Nazir, *Int. J. Biol. Macromol.*, **150**, 861 (2020).
44. M. Y. Han, J. H. Zhang, Y. Y. Hu and R. P. Han, *J. Chem. Eng. Data*, **64**, 3641 (2019).
45. T. Zhou, W. Z. Lu, L. F. Liu, H. M. Zhu, Y. B. Jiao, S. S. Zhang and R. P. Han, *J. Mol. Liq.*, **211**, 909 (2015).
46. E. M. Zong, D. Wei, H. Q. Wan, S. R. Zheng, Z. Y. Xu and D. Q. Zhu, *Chem. Eng. J.*, **221**, 193 (2013).
47. J. W. Lin, X. X. Wang and Y. H. Zhan, *J. Environ. Sci.*, **76**, 167 (2019).
48. X. T. Zhang, R. Z. Zhang, S. S. Chen, K. Wen and R. P. Han, *Desalin. Water Treat.*, **170**, 187 (2019).
49. J. Y. Li, J. Ma, Q. H. Guo, S. L. Zhang, H. Y. Han, S. S. Zhang and R. P. Han, *Water Sci. Technol.*, **81**, 824 (2020).
50. K. Wu, Y. Li, T. Liu, Q. B. Huang, S. J. Yang, W. D. Wang and P. K. Jin, *Appl. Surf. Sci.*, **478**, 539 (2019).